Self-induced Dimensional Reduction and Scaling Transition of mRNA in Polysomes: A Multiscale Simulation Study

Hideki Kobayashi[1] and Horacio V. Guzman*[2]
[1)] *Institute for Computational Physics (ICP), University of Stuttgart, Allmandring 3, 70569 Stuttgart, Germany*
[2)] *Institut de Ciència de Materials de Barcelona ICMAB-CSIC, Campus de la UAB, E-08193 Spain*

(*Electronic mail: hguzman@csic.es)

(*Electronic mail: hideki.kobayashi@icp.uni-stuttgart.de)

(Dated: 31 December 2025)

The spatial architecture and mechanical rigidity of polysomes are crucial determinants of translational efficiency and mRNA stability. In this study, we investigate the conformational statistics of an mRNA backbone decorated with high-density ribosomes using large-scale, extensive molecular dynamics simulations based on the Kremer-Grest bead-spring model. To address the extreme spatial asymmetry between mRNA monomers and ribosomes, we used an efficient tree-based neighbour list algorithm, enabling the analysis of mRNA chains up to $N = 4,969$. Our results demonstrate that the excluded volume of massive ribosomes induces a significant transition in the scaling exponent ν from 0.59 to approximately 0.9. In the conformation of mRNA, this shift translates to a self-induced dimensional reduction from a three-dimensional random coil to a quasi-one-dimensional rigid-rod-like structure. Such a transition is further evidenced by a periodic "regain" of the bond-bond correlation function $C(n)$ at ribosome attachment sites, indicating a geometric alignment absent in standard homopolymers. These findings reveal that the geometric crowding of ribosomes itself provides a robust physical prerequisite for the formation of higher-order polysome architectures, bridging the gap between universal polymer scaling and structural properties of mRNA during translation.

I. INTRODUCTION

The spatial architecture and mechanical rigidity of polysomes, which are complexes formed by multiple ribosomes translating a single mRNA strand, are fundamental determinants of protein synthesis regulation and mRNA stability. Recent cryo-electron tomography studies have revealed that polysomes can adopt sophisticated higher-order structures, such as helical or circular configurations, including the notable "closed-loop" model, among others[1–8]. These structures are thought to optimise translation efficiency and protect genetic information from enzymatic degradation[9–13]. From a physical perspective, the maintenance of these architectures depends critically on the effective stiffness of the mRNA backbone. However, the microscopic origin of this rigidity remains poorly understood, often being reduced to a generic increase in persistence length without a rigorous statistical-mechanical basis.

Ribosome attachment is expected to influence mRNA conformation through two distinct physical mechanisms: (i) the enhancement of local bending rigidity due to the binding of massive protein complexes, and (ii) the global steric exclusion imposed by the large ribosomal volumes. Previous numerical studies, such as those by Fernandes et al.[14], have focused on the former, premising that ribosomal attachment increases the persistence length and thereby determines the mRNA's spatial extent. To isolate these effects, it is helpful to consider a "ghost" ribosome model as a baseline, where appendages increase local stiffness at their attachment points but lack mutual steric repulsion, although in actual cellular environments, ribosomes are bulky structures that are significantly larger than the mRNA strand.

This observation raises a fundamental question we tackle: how does the ribosomal excluded volume affect mRNA during translation? In classical polymer physics, theoretical and experimental work on bottle-brush polymers suggests that flexible side chains merely rescale the backbone's persistence length without altering its scaling exponents[15–17]; any observed shift in ν is typically attributed to finite-size effects rather than a change in the universality class. However, ribosomes, exceeding the mRNA monomer diameter by more than thirty-fold, are not only massive but are also, comparatively, highly rigid macromolecules. We argue that the interplay of extreme asymmetry and rigidity creates collective multi-body interactions among ribosomes that can no longer be mapped onto a single stiffness parameter. These collective interactions construct a "steric corridor" that non-locally restricts the backbone conformational space, potentially shifting the polymer into a different universality class. Conventional models that neglect these interactions risk failing to capture the collective behaviour of the polysome as a supramolecular assembly. Nevertheless, this effect remains unexplored because simulating such extreme asymmetries in the long-chain limit is computationally challenging and demands new modeling schemes.

In this work, we investigate the conformational statistics of mRNA in polysomes by employing the standard Kremer-Grest (KG) bead-spring model[18]. By combining the Weeks-Chandler-Andersen (WCA) and FENE potentials, we strip away chemical specificity to isolate the pure role of geometric constraints. Our focus is on how the spatial asymmetry between mRNA monomers and ribosomes dictates the global scaling behaviour. However, the standard cell list is ill-equipped for the disparate length scales in such a spatially asymmetric system. These conventional approaches face prohibitive computational costs and memory bottlenecks in full-

length mRNA simulations ($N = 4,969$). To overcome these difficulties, we use an efficient tree-based neighbourlist algorithm. Unlike the standard method, the tree-based neighbourlist enables precise, rapid evaluation of steric repulsions across the entire polysome.

Our results demonstrate that the transition of the mRNA backbone toward a quasi-rigid rod regime ($\nu \approx 0.9$) is not merely a consequence of local stiffening, but is fundamentally driven by a "self-induced dimensional reduction" caused by the crowded arrangement of real ribosomal volumes. This geometric alignment serves as a robust foundation for the formation of complex polysome architectures.

II. MODEL AND NUMERICAL METHOD

In this study, we construct a coarse-grained model to simulate the conformational behaviour of a polysome, defined as an mRNA molecule associated with multiple ribosomes. This model aims to capture essential features of polysome organisation and the spatial configuration of mRNA under translationally active conditions.

The mRNA is modelled as a polymer chain using the Kremer–Grest model[18]. Each monomer represents a coarse-grained nucleotide unit and is connected to its neighbours by finitely extensible nonlinear elastic (FENE) bonds:

$$V_{\mathrm{FENE}} = -\frac{1}{2}K_F R_0^2 \left\{ 1 - \left(\frac{r}{R_0} \right)^2 \right\}, \tag{1}$$

where K_F and R_0 stand for the spring constant and the maximum extension of the bond, respectively. Excluded volume interactions between monomers are introduced via the Weeks-Chandler-Andersen potential (WCA):

$$V_{\mathrm{LJ}} = \begin{cases} 4\varepsilon_{\mathrm{LJ}} \left[\left(\frac{\sigma_{\mathrm{m}}}{r}\right)^{12} - \left(\frac{\sigma_{\mathrm{m}}}{r}\right)^{6} \right] + \varepsilon_{\mathrm{LJ}}, & r < r_{\mathrm{c}} \\ 0, & r > r_{\mathrm{c}}, \end{cases} \tag{2}$$

The parameters $\varepsilon_{\mathrm{LJ}}$ and σ_{m} are the strength of the interaction and the diameter of the monomers, respectively. $r_{\mathrm{c}} = 2^{1/6}\sigma_{\mathrm{m}}$ stands for the cutoff length of potential. The total number of monomers in the mRNA chain is represented by N. The simulations are performed with the following chain lengths: $N = 2000, 3000, 4060, 4969$. The diameter of each monomer is defined as the unit length $u = 0.6nm$ in real space, and all physical quantities are expressed in reduced units based on this length. The energy unit is $k_B T$, and the mass unit corresponds to the mass of a monomer.

We use a bending-angle potential to introduce chain stiffness and control mRNA flexibility. This potential acts on every triplet of consecutive monomers, imposing a preferred bending angle θ_0 using a harmonic angle potential:

$$V_{\mathrm{BEND}} = \frac{1}{2}K_{\mathrm{B}} \left(\theta - \theta_0\right)^2, \tag{3}$$

In our simulations, we consider $\theta_0 = \pi/2$ and $2\pi/3$ to mimic various structural constraints[19].

Each ribosome is modeled as a pair of spheres representing the small and large subunits, with diameter $\sigma_{\mathrm{S}} = 20u$, and $\sigma_{\mathrm{L}} = 30u$ (i.e., $12\,nm$ and $18\,nm$). When these two spheres are in contact, the resulting composite structure spans a long-axis length of 30 nm in real space. This value is about 20˘30% larger than experimentally observed bacterial ribosome sizes ($20 - 25\,,nm$). However, this discrepancy is compensated for by a later correction described below.

Each ribosome binds to the RNA at a fixed segment of 30 monomers, which are harmonically constrained to the surface of the small subunit. The harmonic potential is applied to enforce attachment, using a spring constant $k = 10$. One of the centre monomers of this 30-monomer segment is additionally connected to the centre of the large subunit via another harmonic potential of the same spring constant $k = 10$, with an equilibrium distance of $10u$. This construction ensures that the two subunits behave as a single functional ribosome. Due to the extended connection between the monomers and the large subunit, the effective long-axis length of the ribosome becomes approximately $45u$ (27 nm), while the short-axis length remains 18 nm. Although this is still somewhat larger than experimental ribosome dimensions, the short-axis alignment matches typical bacterial sizes, and we consider this acceptable within a coarse-grained framework.

Multiple ribosomes are attached to the mRNA chain to form polysomes, with the spacing between adjacent ribosomes controlled at intervals of $30 \times N_{\mathrm{space}}$. One of the centre monomers of this 30-monomer segment is additionally connected to the centre of the large subunit via another harmonic potential of the same spring constant $k = 10$, with an equilibrium distance of $10u$, to examine how variations in ribosome spacing affect RNA conformation and the overall geometry of polysomes.

All large particles (ribosomal subunits) interact via a Gaussian Core (GCP), which provides soft, long-ranged repulsion. The strength of the Gaussian potential is set to 5 for ribosome–ribosome interactions and 10 for ribosome–monomer interactions. The choice of a soft repulsive potential over a hard-core potential (e.g., WCA) is motivated by two factors. First, from a physical perspective, the interaction strength $A = 10$ provides a sufficiently high energy barrier to prevent significant overlap under physiological densities, effectively maintaining the "steric corridor" described in the Introduction. Second, from a computational standpoint, the GCP avoids the numerical instabilities and unphysical large forces that often arise in highly asymmetric systems (30:1 size ratio) when a monomer occasionally penetrates a hard-core shell. The potential is truncated and shifted to smoothly vanish at a cut-off radius set to 120% of the sum of the interacting particles' radii. The standard deviation σ of the Gaussian potential is defined as the sum of the radii of the two interacting particles:

$$\sigma_{ij} = r_i + r_j = \frac{\sigma_i + \sigma_j}{2}. \tag{4}$$

The Gaussian Core Potential is defined as follows:

$$V_{\mathrm{GC}}(r_{ij}) = A \exp\left(-\frac{r_{ij}^2}{2\sigma_{ij}} \right), \tag{5}$$

where A is the strength of the potential. To ensure that the Gaussian potential vanishes smoothly at the cutoff radius r_c, we introduce a smoothing function $S(r_{ij})$, which continuously reduces the interaction strength to zero as $r_{ij} \to r_c$. The modified Gaussian Core Potential is defined as:

$$V_{\mathrm{GC}}(r_{ij}) = A \exp\left(-\frac{r_{ij}^2}{2\sigma_{ij}^2}\right) \cdot S(r_{ij}), \tag{6}$$

where $S(r_{ij})$ is a smoothing function that satisfies $S(r_{ij}) = 1$ for $r_{ij} \ll r_c$ and decays smoothly to zero as $r_{ij} \to r_c$. We used the form of the smoothing function defined as:

$$S(r_{ij}) = \frac{(r_c^2 - r^2)^2 (r_c^2 + 2r^2 - 3r_s^2)}{(r_c^2 - r_s^2)^3}, \tag{7}$$

where $r_s = 1.1 \times (r_i + r_j)$ is the start of the smoothing region, and r_c is the cutoff radius, set to $1.2 \times (r_i + r_j)$. This approach ensures a smooth truncation of the potential and its derivative, improving the numerical stability of simulations.

A key feature of this system is the coexistence of interaction potentials with vastly different length scales. While monomer-monomer WCA interactions act over a short range ($r_c \approx 1.12u$), ribosome-ribosome Gaussian interactions extend up to $r_c \approx 36u$ (for $\sigma_{\mathrm{L}} = 30u$). In a standard cell-list algorithm, the cell size is determined by the largest interaction range, leading to an $O(r_c^3)$ increase in the number of particles per cell and prohibitive computational overhead.

To overcome this scale disparity, we employ a tree-based neighbour list algorithm[20,21] implemented in HOOMD-blue[22]. This hierarchical approach decouples the search scales, allowing for efficient neighbour identification even when the interaction radii differ by a factor of 30. All simulations were accelerated using A100 and H100 GPUs, enabling us to reach the long-chain limit ($N = 5,000$) within reasonable wall-clock times.

We set the parameters $K_{\mathrm{F}} = 30, R_0 = 1.5, \varepsilon_{\mathrm{LJ}} = 1.0, K_{\mathrm{B}} = 50.0$ and $dt = 0.002$.

Using the model described above, we evaluate its structural properties via NVT molecular dynamics (MD) simulation with a Langevin thermostat at $k_{\mathrm{B}}T = 1$ and friction coefficient $\Gamma = 0.1$. We calculate eight independent polysomes at the system size $L = 1000u$ to obtain the structural properties.

This modelling framework allows us to systematically investigate how periodic ribosome binding affects mRNA conformation under various geometric constraints. The use of soft repulsive potentials enables the simulation of crowded polysomes-like conditions without hard-core overlap, while harmonic constraints impose realistic tethering of RNA to ribosomal subunits. The angle potential allows us to tune RNA stiffness and assess its impact on large-scale structure formation. Altogether, this modelling framework provides a minimal yet physically informed platform for systematically exploring RNA organisation in the context of active translation.

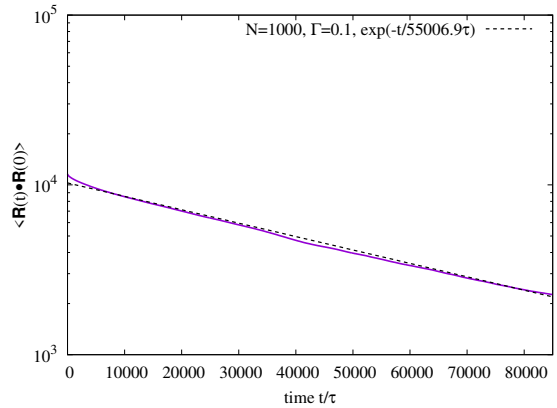

FIG. 1. End-to-end vector autocorrelation function $\langle \mathbf{R}_{\mathrm{E}}(t) \cdot \mathbf{R}_{\mathrm{E}}(0) \rangle$ for $N = 1000$ (solid line). It is proportional to $\exp[-t/(55006.9\tau)]$ (dashed line).

III. RESULTS

To ensure that the systems are properly equilibrated, we estimate the characteristic relaxation time of a system. Specifically, we calculated the time-displaced autocorrelation function of the end-to-end vector, $\langle \mathbf{R}_{\mathrm{E}}(t) \cdot \mathbf{R}_{\mathrm{E}}(0) \rangle$, for $N = 1000$ and $N_{space} = 5$, where $\mathbf{R}_{\mathrm{E}} = \mathbf{r}_N - \mathbf{r}_1$. As shown in Fig. 1, this function can be well approximated by an exponential decay,

$$\langle \mathbf{R}_{\mathrm{E}}(t) \cdot \mathbf{R}_{\mathrm{E}}(0) \rangle \propto \exp\left(-\frac{t}{\tau_{\mathrm{dec}}}\right), \tag{8}$$

where the data indicate $\tau_{\mathrm{dec}} \approx 55000\tau = 0.55\Gamma N^2 \tau$. This corresponds to approximately 16 τ_R, where τ_R is the Rouse relaxation time of a corresponding flexible chain [23], i.e. naked RNA. While the attachment of ribosomes significantly slows down the conformational dynamics, we conclude that equilibration over a time $\tau_{\mathrm{eq}} = 3\tau_{\mathrm{dec}}$ is sufficient (note $\exp(-3) \approx 0.05$).

To determine the scaling exponent ν, we first examine the mean-square end-to-end distance $\langle R_{\mathrm{E}}^2 \rangle$ for two baseline cases: the naked mRNA and the mRNA associated with "ghost" ribosomes. In the ghost-ribosome model, the monomers are constrained to the ribosomal surface as described in the Methods, but all repulsive interactions involving the ribosomal subunits are switched off. As shown in Fig. 2(Left), the naked mRNA—representing the standard KG model with a bending potential—yields $\nu \approx 0.6$. This is consistent with the expected scaling for a self-avoiding walk in a good solvent and agrees with previous studies employing the KG model with angular constraints[24]. For the mRNA with ghost ribosomes, the scaling exponent remains $\nu \approx 0.6$, indicating that the local structural constraint imposed by the ribosome binding sites does not fundamentally affect the fractal dimension of the polymer at large length scales. However, it should be noted that the absolute magnitude of $\langle R_{\mathrm{E}}^2 \rangle$ for the ghost-ribosome system is larger than that for the naked mRNA at any given N. This chain expansion can be attributed to the local stiffening and the spatial occupancy of the binding segments, which ef-

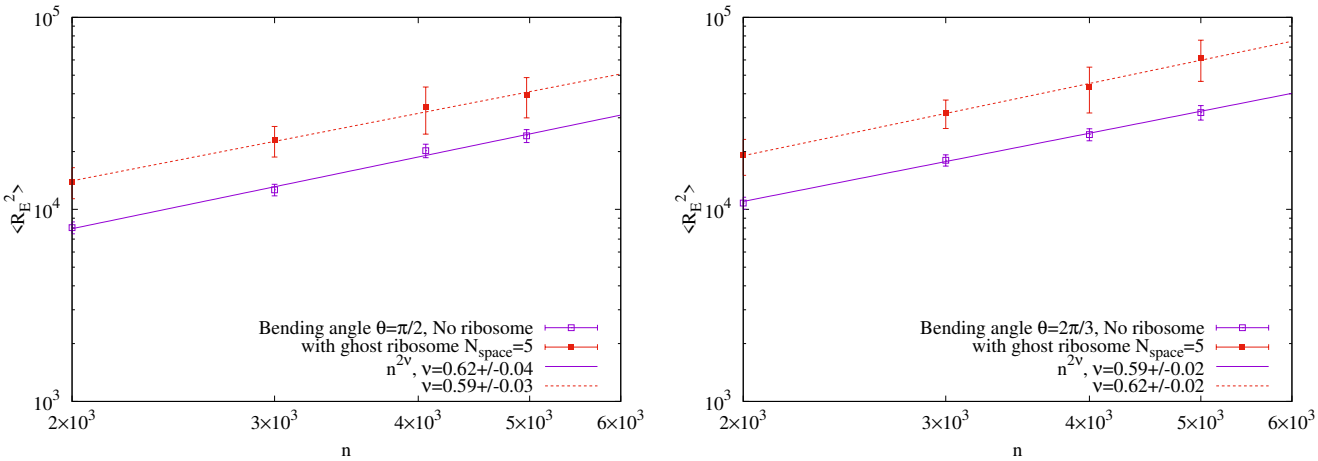

FIG. 2. Mean square end-to-end distance R_{E}^2 as a function of monomer number N for no-ribosome (open square) and ghost-ribosome with $N_{\mathrm{space}} = 5$ (close square). Solid and dashed lines represent least-squares fits to $n^{2\nu}$. Left: The bending angle $\theta = \pi/2$. Right: $\theta = 2\pi/3$

fectively increase the Kuhn length of the chain. These baseline results can be well understood through the blob picture[25], where the ghost ribosomes act as local perturbations that renormalise the persistence length without shifting the global universality class of the self-avoiding-walk (SAW). Similar results and analysis apply for Fig. 2(Right), where the bending angle is $\theta = 2\pi/3$.

In contrast, as shown in Fig. 3, the mRNA associated with "real" ribosomes, incorporating repulsive Gaussian core interactions, exhibits a scaling exponent ν significantly larger than the SAW value. This result is particularly notable; from a naive perspective, one might expect that the repeating units of ribosomes and their intervening sub-chains would merely act as renormalised blobs, thereby preserving the SAW universality class ($\nu \approx 0.6$).

For $\theta = \pi/2$, we find $\nu \approx 0.7$, which clearly exceeds the three-dimensional SAW value. According to the Flory-type relation $\nu = 3/(d_{\mathrm{eff}} + 2)$, this shift corresponds to a reduction in the effective dimensionality d_{eff} from 3 to approximately 2.3. We suggest that the presence of the massive ribosomal volumes restricts the available conformational space for the mRNA backbone, effectively "squeezing" the chain into a lower-dimensional manifold.

Furthermore, for $\theta = 2\pi/3$, the scaling exponent increases to $\nu = 0.91 \pm 0.08$ for $N_{\mathrm{space}} = 5$ and 0.83 ± 0.07 for $N_{\mathrm{space}} = 11$. This indicates that the angular constraint, which promotes a more extended chain, works in interplay with the ribosomal excluded volume to reduce d_{eff}, driving the system toward the rigid-rod limit ($\nu \to 1$). Crucially, for the $N_{\mathrm{space}} = 11$ case, the averaged distance between ribosomes is larger than the interaction range of the Gaussian core potential ($36u$). Specifically, for $\theta = \pi/2$, the mean inter-ribosomal distance is $42.6u$ (based on $\langle R_{\mathrm{E}}^2 \rangle = 0.51 N^{1.41}$ at the sub-chain length $N = 30 N_{\mathrm{space}} = 330$), while for $\theta = 2\pi/3$, it is $36.5u$ ($\langle R_{\mathrm{E}}^2 \rangle = 0.08 N^{1.67}$). These results, particularly for the $\theta = 2\pi/3$ case, imply that the increase in ν is not driven by direct ribosome-ribosome repulsion. Instead, it originates from a global change in the effective dimensionality d_{eff} imposed by the ribosomal presence along the mRNA strand.

To validate the scaling exponent ν through an independent physical property, we calculate the static structure factor $S(q)$ of the mRNA chain:

$$S(q) = \frac{1}{N} \sum_{i,j} \left\langle \frac{\sin(q r_{ij})}{q r_{ij}} \right\rangle, \tag{9}$$

where q denotes the magnitude of wave vector and r_{ij} is the distance between the i-th and j-th monomers. Note that the coordinates of the ribosomal subunits are excluded from this calculation to focus solely on the statistical properties of the mRNA backbone.

According to polymer scaling theory[25,26], the structure factor follows a power-law decay $S(q) \propto q^{-1/\nu}$ in the fractal regime, defined by the conditions $qR_g \gg 1$. This relationship allows for a direct comparison between the scaling exponents ν obtained from the real-space distance R_{E}^2 and the reciprocal-space structure factor $S(q)$.

First, we examine $S(q)$ for the ghost ribosome system with $\theta = \pi/2$, $N_{\mathrm{space}} = 5$ and $N = 4969$, as shown in Fig. 4. At intermediate wave vectors ($0.03 < q < 0.3$), the emergence of plateaus and subtle fluctuations indicates a localised departure from self-similarity, reflecting the structural correlations within ribosome-constrained segments. Since our primary interest lies in the global statistical properties of the mRNA backbone, we performed a power-law fit, $S(q) = A q^{-1/\nu}$, within the range $0.4 < q < 2$. In this interval, the aforementioned local structural correlations become negligible, and $S(q)$ exhibits consistent fractal scaling over nearly a decade of the wave vector. Furthermore, this range satisfies the condition $qR_g \gtrsim 20$ (estimated using $R_g^2 \approx R_{\mathrm{E}}^2/6 \approx 6667$).

The fit yields $\nu = 0.61 \pm 0.01$, showing good agreement with the data over the broad range of $0.1 < q < 3$. This result confirms that, in the absence of ribosomal-excluded-volume interactions, the mRNA maintains the SAW universality class. Notably, this exponent is consistent with previous studies of SAW chains on simple cubic lattices with a bending potential $\varepsilon_b(1 - \cos\theta)$ for $\varepsilon_b < 5$[27].

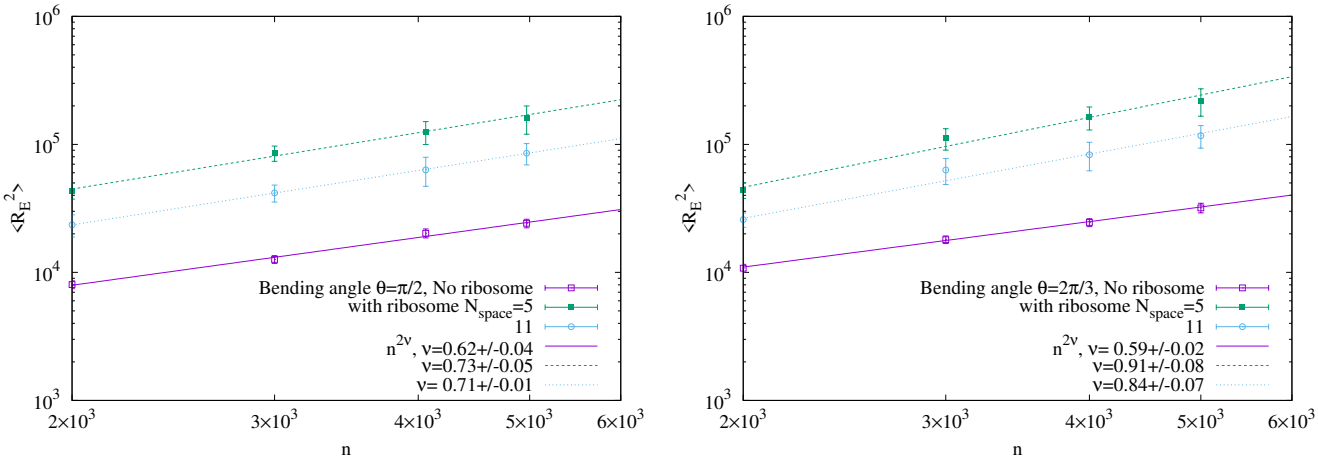

FIG. 3. Mean square end-to-end distance R_E^2 as a function of monomer number N for no ribosome (open squares), real ribosome with $N_{\text{space}} = 5$ (closed squares) and $N_{\text{space}} = 11$ (open circle). Solid, dashed and dotted lines represent least-squares fits to $n^{2\nu}$. Left: The bending angle $\theta = \pi/2$. Right: $\theta = 2\pi/3$

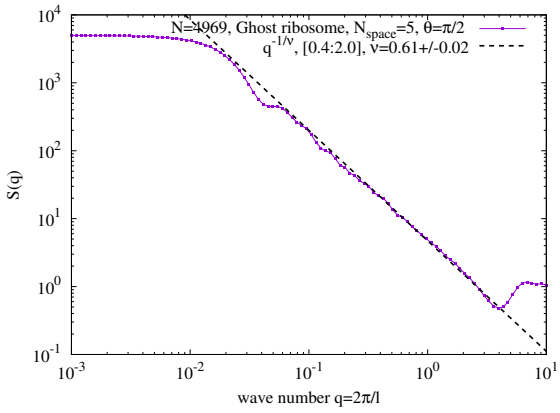

FIG. 4. Structure factor $S(q)$ for ghost ribosomes with $\theta = \pi/2$, $N = 4969$, and $N_{\text{space}} = 5$. The dashed line shows a least-squares fit to $q^{-1/\nu}$, yielding $\nu = 0.61 \pm 0.02$.

In the presence of explicit ribosomal excluded volume interactions, the mRNA chain exhibits a distinctive multiscale scaling behaviour in its structure factor $S(q)$. Figure 5 (Left) shows $S(q)$ for $\theta = \pi/2$ with $N_{\text{space}} = 5$ and 11. Remarkably, both systems show almost identical behaviour in the fractal regime, indicating that the observed structural modulation of the backbone is robust against changes in ribosome density.

For the intermediate scale ($0.4 < q < 1.0$), after the direct structural interference from ribosome insertion and ribosome-ribosome repulsions has subsided, we obtain a scaling exponent of $\nu = 0.66 \pm 0.01$ for both N_{space} cases. This value is significantly higher than the one observed in the ghost-ribosome system ($\nu = 0.61 \pm 0.01$), providing direct evidence that the ribosomal excluded volume effectively reduces the available conformational space, leading to an inherently more extended chain through effective dimensional reduction.

It is noteworthy that for $N_{\text{space}} = 5$, a broader fit starting from lower q ($q > 0.15$) yields a higher apparent exponent of $\nu \approx 0.72 \pm 0.02$. This enhancement reflects a combination of the aforementioned statistical dimensional reduction and the explicit geometric "pushing" induced by long-range excluded-volume correlations between ribosomes. In contrast, for the case of $N_{\text{space}} = 11$, the structure factor in this low-q regime ($q < 0.4$) is dominated by more pronounced structural interference and plateaus arising from the ribosomal arrangement. Because these local correlations obscure the underlying scaling behaviour, we refrain from applying the power-law fit in the $q < 0.4$ region for $N_{\text{space}} = 11$. This ensures that our determination of the scaling exponent remains focused on the universal backbone statistics rather than being biased by the ribosomes' specific insertion geometry.

Finally, in the high-q regime ($1.0 < q < 3.0$), the exponent reverts to $\nu = 0.61 \pm 0.01$, consistent with the universal SAW behaviour. This separation of scales clearly demonstrates that, while the ribosomal network globally stretches the mRNA strand through both geometric and statistical constraints, the intrinsic polymer statistics are preserved at the sub-chain level.

Figure 5 (Right) shows $S(q)$ for the system with a more restricted bending angle, $\theta = 2\pi/3$, at $N_{\text{space}} = 5$ and 11. Similar to the $\theta = \pi/2$ case, both systems exhibit almost identical behaviour in the fractal regime regardless of N_{space}. However, their scaling characteristics differ fundamentally from those observed at $\theta = \pi/2$.

For $\theta = 2\pi/3$, in the intermediate scale ($0.4 < q < 1.0$) where ribosomal interference is negligible, we obtain a scaling exponent of $\nu = 0.71 \pm 0.01$ for both N_{space} cases. This value is not only significantly higher than that of the ghost-ribosome system ($\nu = 0.61 \pm 0.01$) but also exceeds the value for the $\theta = \pi/2$ system ($\nu = 0.66 \pm 0.01$). Surprisingly, even when fitting in the higher-q range ($1.0 < q < 2.0$), the exponent remains high at $\nu \approx 0.7$. This persistent scaling indicates that the mRNA is no longer a standard SAW chain and instead behaves as a quasi-rigid rod, suggesting a fundamental change in the intrinsic polymer statistics at this angle.

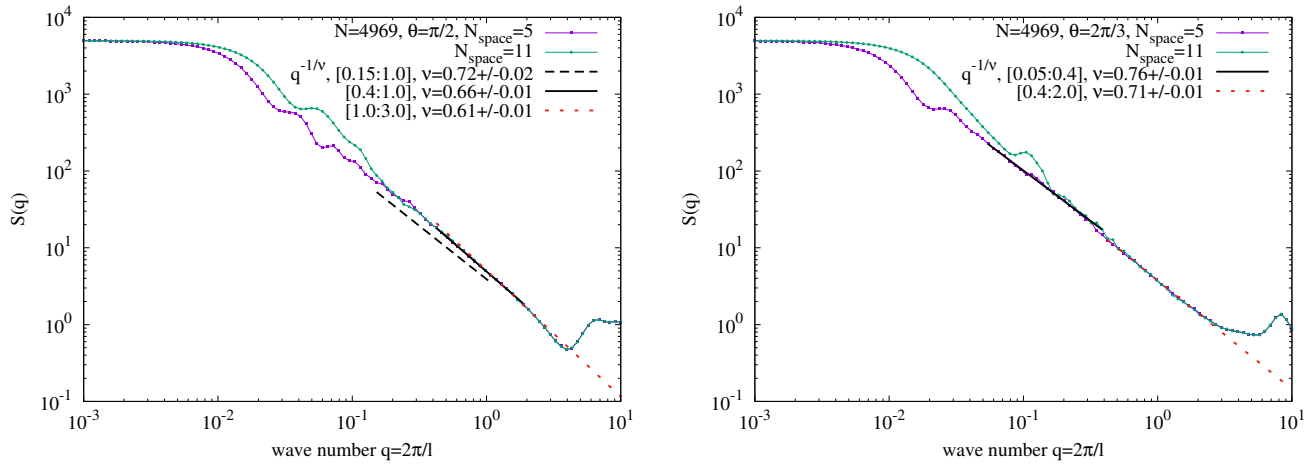

FIG. 5. Structure factor $S(q)$ for real ribosomes with $N = 4969$ and $N_{\text{space}} = 5(\text{square}), 11(\text{circle})$. The solid, dashed and dotted line shows a least-squares fit to $q^{-1/\nu}$. Left: The bending angle $\theta = \pi/2$. Right: $\theta = 2\pi/3$

We consider that this transition is driven by the interplay between the geometric constraints imposed by the bending angles and the ribosomes' spatial occupancy. The restrictive bending angle confines the bond directions within a narrower cone, which further enhances the reduction of the effective dimension d_{eff}. Although fluctuations exist in the low-q region ($0.05 < q < 0.4$), a broader fit yields $\nu = 0.76 \pm 0.01$, similar to the "pushing" effect seen in $\theta = \pi/2$. These results suggest that while the mechanism for increasing ν is essentially the same as in the $\theta = \pi/2$ case, the increased angular constraint pushes the system into a qualitatively different regime of polymer statistics.

To confirm the enhanced confinement of bond orientations in the presence of real ribosomes, we calculate the bond-bond correlation function $C(n)$ strictly within the sub-chain segments between two neighbouring ribosomes:

$$C(n) = \frac{1}{N_{\text{sub}} - n} \sum_{i=1}^{N_{\text{sub}}-n} \langle \mathbf{l}_{i+n} \cdot \mathbf{l}_i \rangle, \tag{10}$$

where N_{sub} is the number of bonds in a sub-chain (defined as $N_{\text{sub}} = 30(N_{\text{space}} - 1)$ in our model), and $\mathbf{l}_i = \mathbf{r}_{i+1} - \mathbf{r}_i$ is the i-th bond vector. The summation is restricted to pairs of bonds belonging to the same segment between two consecutive ribosomes.

It is well known that for a simple freely rotating chain (FRC), $C(n)$ is characterised by a single characteristic length, resulting in a simple exponential decay: $C(n) = \sigma^2 \exp[n \log(\langle \cos\theta \rangle)]$. In contrast, our KG model, even in the ghost-ribosome system, exhibits more complex behaviour in the short-range regime due to excluded-volume interactions between monomers, which introduce multiple length scales.

For a swollen polymer chain in the long-range regime, $C(n)$ is expected to follow the universal scaling relation $C(n) \propto n^{2(\nu-1)}$[28–30]. If the real ribosomes effectively restrict the bond orientations, $C(n)$ is expected to show a significantly slower decay (corresponding to a larger ν) compared to the ghost-ribosome system.

Note that, because this analysis is performed within finite-sized sub-chains, a simple power-law decay may not hold over the entire range. As n approaches the sub-chain length N_{sub}, the geometric boundary conditions, where the ends of the chain are tethered to the ribosomes, become dominant. We consider that this confinement will cause the correlation to deviate upward from the power-law decay, eventually exhibiting a "regain" of correlation. Such a departure from standard polymer statistics provides direct evidence that the ribosomal arrangement forces the mRNA strand to transition from a random-walk-like distribution to a more ordered, quasi-rod-like structure within the inter-ribosomal space.

Figure 6(Left) shows $C(n)$ for $\theta = \pi/2$ with $N_{\text{space}} = 5$ and 11. In the small-n regime ($n < 10$), all systems exhibit strong oscillations. Specifically, $C(1) \approx 0.02$, consistent with the bending potential, while $C(2)$ jumps to approximately 0.3, followed by a gradual decay with oscillations up to $n \approx 7$. This oscillation originates from local excluded-volume correlations and the associated entropic effects. In a configuration where $\mathbf{l}_{i+2} = -\mathbf{l}_i$, the possible orientations for the subsequent bond $\mathbf{l}_{i+3}$ are severely restricted to avoid steric overlaps with the preceding segments (notably $\mathbf{l}_i$), while still maintaining the bending angle constraint of $\pi/2$. This significant reduction in the number of accessible microstates leads to a substantial loss of conformational entropy. To avoid such an entropic penalty, the system statistically suppresses the $\mathbf{l}_{i+2} \approx -\mathbf{l}_i$ state, effectively forcing $\mathbf{l}_{i+2}$ to point away from $-\mathbf{l}_i$. This mechanism results in the pronounced positive correlation at $n = 2$ and the characteristic oscillatory profile in the short-range correlation.

In the large-n regime, the behaviour differs markedly between systems. For ghost ribosomes, $C(n)$ exhibits a monotonic power-law decay with $\nu = 0.56 \pm 0.02$, consistent with previous SAW studies. In contrast, real ribosome systems exhibit a plateau followed by a regain of correlation. The plateau begins at $n \approx 20$ for $N_{\text{space}} = 5$ and $n \approx 100$ for $N_{\text{space}} = 11$. The regain of correlation is observed from $n \approx 100$ for $N_{\text{space}} = 5$ and $n \approx 200$ for $N_{\text{space}} = 11$. Before the plateau, $C(n)$ follows a power law with $\nu = 0.70 \pm 0.01$, indicating

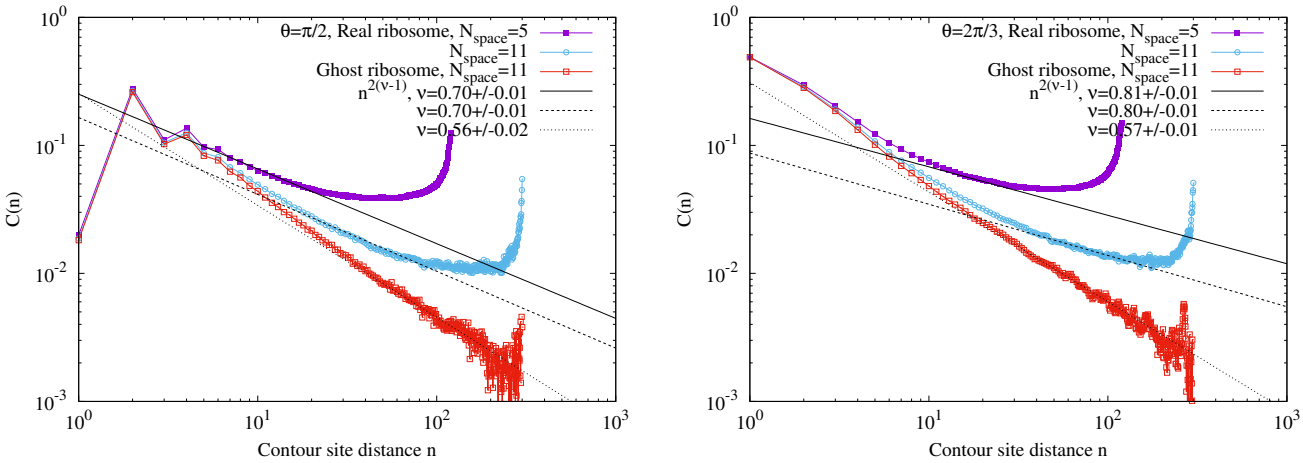

FIG. 6. Bond-bond correlation function $C(n)$ vs. contour site distance n for real ribosomes with $N_{\text{space}} = 5$ (closed squares) and 11 (open circles), and ghost ribosomes with $N_{\text{space}} = 11$ (open squares). Solid, dashed, and dotted lines represent least-squares fits to $n^{2(\nu-1)}$. Left: $\theta = \pi/2$. Right: $\theta = 2\pi/3$.

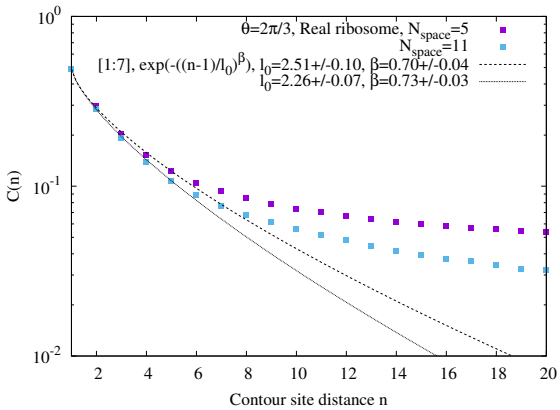

FIG. 7. Semi-log plot of the bond-bond correlation function $C(n)$ vs. contour site distance n for real ribosomes at $\theta = \pi/2$ with $N_{\text{space}} = 5$ (open squares) and 11 (open circles). Lines represent least-squares fits to $\exp\{-[(n-1)/l_p]^{\beta}\}$. For $N_{\text{space}} = 5$, $l_p = 2.51$ and $\beta = 0.70$ (dotted line); for $N_{\text{space}} = 11$, $l_p = 2.26$ and $\beta = 0.73$ (dashed line).

significant stretching.

For $\theta = 2\pi/3$, $C(n)$ exhibits qualitatively similar behavior but with a larger scaling exponent, $\nu = 0.78 \pm 0.01$, in the mid-range (Fig. 6, Right), which is in excellent agreement with the global stretching observed in R_{E}^2 and $S(q)$.

To investigate the short-range behaviour of the $\theta = 2\pi/3$ system, Fig. 7 presents a semi-log plot of $C(n)$. The non-linear decay indicates that the correlation deviates from a simple exponential form. Instead, the data are well-described by a stretched exponential function, $\exp\{-[(n-1)/l_p]^{\beta}\}$, which can be interpreted as a superposition of relaxation processes:

$$\exp\left[-\left(\frac{n-1}{l_p}\right)^{\beta}\right] = \int_0^{\infty} \rho(u) \exp\left(-\frac{n-1}{u}\right) du, \quad (11)$$

where l_p represents the characteristic persistence length and β is the stretching exponent. This form implies a distribution $\rho(u)$ of local persistence lengths, where a decrease in β from unity indicates a broader distribution. The explicit form of $\rho(u)$ is given in Eqs. (23) and (24) of Ref.[31]. Our fitting yields $l_p = 2.51$ and $\beta = 0.70$ for $N_{\text{space}} = 5$, and $l_p = 2.26$ and $\beta = 0.73$ for $N_{\text{space}} = 11$. The smaller β for $N_{\text{space}} = 5$ suggests that a higher density of ribosomes induces more pronounced local structural heterogeneity in the mRNA backbone.

These results microscopically substantiate the reduction of the effective dimension of the mRNA. The slower decay and the regain of correlation demonstrate that ribosomal excluded volume effectively funnels the chain's conformational space, forcing it into a quasi-rod-like alignment between ribosomal nodes. In addition, our results clearly demonstrate that the presence of real ribosomes leads to a much slower decay of bond correlations. Moreover, the regain of $C(n)$ as n approaches the boundaries of the sub-chain indicates that the bond orientations are geometrically constrained to align with the axis connecting the ribosomes. This provides direct, microscopic evidence for the reduction of the effective dimension of the mRNA backbone, consistent with the global stretching observed in R_{E}^2 and $S(q)$.

IV. DISCUSSION

The striking result of this study is that the attachment of massive ribosomal constraints fundamentally alters the scaling behaviour of the mRNA backbone, driving the scaling exponent ν toward the quasi-rigid rod limit ($\nu \approx 0.9$). It is important to distinguish this from previous numerical studies[32], which reported that ν can reach values near 0.8 in bead-spring models using long-ranged Gaussian core potentials, where the interaction range is 4 times the bead diameter in the longest case. Despite the apparent similarity in the increase of ν, the underlying physics in our system is qualitatively different. In such models, the increase in ν originates from enhanced inter-

nal stiffness due to direct, long-range bead-bead repulsion. In contrast, our model relies on short-ranged monomer interactions (WCA). Even with modest-ranged Gaussian core potentials, at an interaction range of 1.2 times the ribosome diameter, the observed increase in ν arises from a global reduction in the effective dimensionality d_{eff} imposed by the massive ribosomal volumes. This is microscopically substantiated by the "regain" of bond-bond correlations $C(n)$ at intervals corresponding to neighbouring ribosomes, which is absent in standard homopolymer models, confirming that the ribosomal arrangement funnels the mRNA into a quasi-rod-like alignment.

Experimental observations have established that ribosome or protein binding induces RNA stiffening and structural stabilisation[33,34]. While it may seem intuitive that attaching ribosomes extends the RNA chain by increasing its effective persistence length, our results reveal a more profound mechanism. For instance, numerical work by Fernandes et al.[14], which examines mRNA recycling rates, assumes that ribosomal attachment enhances the mRNA's persistence length. This assumption is physically equivalent to our "ghost-ribosome" system, in which appendages only provide local rigidity without mutual interference. From our findings, we already know that, in a system with real ribosomes, the expansion mechanism is fundamentally different. The observed significant extension is not driven by a simple increase of persistence length, but by the reduction of d_{eff} due to multi-body excluded volume effects.

The stiffening mechanism tackled in this work must be distinguished from the classical confinement effects reported in the literature. Standard scaling theories for polymers in confined geometries, such as nanoslits or cylindrical pores[35–37], rely on *static, external boundary conditions* in which a rigid wall restricts the conformational space. In contrast, the dimensional reduction in our polysome model is *self-induced and internal*. Here, the confinement is dynamically generated by the excluded volume of the ribosomes, which are bulky appendages tethering themselves to the mRNA chain. Notably, our system achieves a nearly 1D limit ($\nu \approx 0.9$) without any physical walls. This suggests that the extreme spatial asymmetry creates an "steric corridor" along the chain's backbone, representing a distinct class of polymer statistics in which the "wall" and the "chain" form a single dynamical entity.

Although our current mRNA-Ribosome model can not reproduce some complex helical or circular configurations observed in cryo-ET studies[9], we are working on extending our model for circular configurations. The formation of higher-order architectures requires anisotropic interactions between ribosomal subunits or specific constraints imposed by the exit tunnel. Nevertheless, this work demonstrates that the geometric stretching of mRNA is a robust physical prerequisite for any such ordering. By showing that mRNA stiffening is an unavoidable consequence of ribosomal crowding, this study bridges the gap between universal polymer scaling and the structure of mRNA-Ribosomes machinery during translation. This multiscale phenomenon, made accessible by the tree-based neighbour list algorithm, underscores the importance of accounting for large-scale geometric constraints in the study of cellular supramolecular assemblies.

V. CONCLUSION

In this study, we have combined a high-performance tree-based neighbour list algorithm with large-scale coarse-grained molecular dynamics simulations to elucidate the conformational statistics of mRNA within a polysome. By modelling the system with a high degree of spatial asymmetry ($N = 4969$ for the backbone and ribosomes of realistic volumes), we identified a fundamental transition in the polymer's scaling behaviour that had previously been overlooked due to modelling and computational limitations. Understanding polysome structural properties constitutes a starting point for further understanding of recent Cryo-ET imaging of polysomes in different environments.

Our findings lead to the following key physical insights: (i) the attachment of ribosomes drives the mRNA backbone into a quasi-rigid rod regime, characterised by a scaling exponent of $\nu \approx 0.9$. This exceeds the predictions of previous average-field or "ghost-ribosome" models, which considered only local increases in persistence length; (ii) the stiffening is not an intrinsic property of the chain but is a *self-induced dimensional reduction*. The multi-body excluded-volume interactions between adjacent, bulky ribosomes effectively funnel the mRNA into a quasi one-dimensional "steric corridor" mimicking the effects of external nanoscale confinement without static walls; (iii) the unique periodic "regain" of the bond-bond correlation function $C(n)$ serves as a structural fingerprint of this transition. It proves that ribosomes act as geometric orientation guides, resetting the chain's alignment and maintaining long-range order. While our minimal mRNA-Ribosome model focuses on equilibrium excluded-volume effects, it provides a necessary physical foundation for understanding the complex architectures of polysomes. The discovery that ribosomal crowding itself is sufficient to induce a nearly one-dimensional mRNA structure offers a new perspective on how genetic information is physically organised for efficient translation.

Finally, the success of the tree-based neighbour list in handling extreme spatial/size asymmetries opens new avenues for simulating other crowded supramolecular assemblies, such as protein-DNA or protein-RNA complexes. Our work demonstrates that, at the cellular level, large-scale geometric constraints could supersede local chemical details, providing a novel interpretation of polysome organisation.

ACKNOWLEDGMENTS

We thank Tatsuhisa Tsuboi for illuminating discussions on the experimental measurements of mRNA during translation. H.K. thanks Gemini 3 for its assistance with grammatical correction and prose flow, both of which were subsequently reviewed and approved by the authors. H.V.G. acknowledges financial support from the Ramón y Cajal grant No. RYC2022-038082-I and Spanish Ministry of Science and Innovation, through project PID2023-150536NA-I00, and the "Severo Ochoa" Grant No. CEX2023-001263-S for Centers of Excellence; and CSIC's grant MMT24-ICMAB-01 for the

nanoML4Med project. H.V.G. acknowledges also Red Española de Supercomputación (RES) for the computing time and technical support at the Finisterrae III supercomputer projects FI-2025-2-0058 and Marenostrum 5 FI-2025-3-0049. The authors are also deeply grateful to Kurt Kremer for years of fruitful collaborations and scientific discussions, in particular on the topic of efficient methods for multiscale simulations.

[1] A. Jacobson, "Poly (a) metabolism and translation: the closed-loop model." Translational control. , 451–480 (1996).

[2] A. Jacobson and S. W. Peltz, "Interrelationships of the pathways of mrna decay and translation in eukaryotic cells," Annual review of biochemistry **65**, 693–739 (1996).

[3] A. G. Myasnikov, Z. A. Afonina, J.-F. Ménétret, V. A. Shirokov, A. S. Spirin, and B. P. Klaholz, "The molecular structure of the left-handed supra-molecular helix of eukaryotic polyribosomes," Nature communications **5**, 5294 (2014).

[4] Z. A. Afonina, A. G. Myasnikov, V. A. Shirokov, B. P. Klaholz, and A. S. Spirin, "Formation of circular polyribosomes on eukaryotic mrna without cap-structure and poly (a)-tail: a cryo electron tomography study," Nucleic acids research **42**, 9461–9469 (2014).

[5] T. N. Baymukhametov, D. N. Lyabin, Y. M. Chesnokov, I. I. Sorokin, E. V. Pechnikova, A. L. Vasiliev, and Z. A. Afonina, "Polyribosomes of circular topology are prevalent in mammalian cells," Nucleic acids research **51**, 908–918 (2023).

[6] H. Xing, R. Taniguchi, I. Khusainov, J. P. Kreysing, S. Welsch, B. Turoňová, and M. Beck, "Translation dynamics in human cells visualized at high resolution reveal cancer drug action," Science **381**, 70–75 (2023).

[7] W. Zheng, Y. Zhang, J. Wang, S. Wang, P. Chai, E. J. Bailey, C. Zhu, W. Guo, S. C. Devarkar, S. Wu, *et al.*, "Visualizing the translation landscape in human cells at high resolution," Nature Communications **16**, 10757 (2025).

[8] Y.-T. Chang, B. A. Barad, J. Hamid, H. Rahmani, B. M. Zid, and D. A. Grotjahn, "Cytoplasmic ribosomes on mitochondria alter the local membrane environment for protein import," Journal of Cell Biology **224**, e202407110 (2025).

[9] F. Brandt, L.-A. Carlson, F. U. Hartl, W. Baumeister, and K. Grünewald, "The three-dimensional organization of polyribosomes in intact human cells," Molecular cell **39**, 560–569 (2010).

[10] Q. Vicens, J. S. Kieft, and O. S. Rissland, "Revisiting the closed-loop model and the nature of mrna 5'-3' communication," Molecular cell **72**, 805–812 (2018).

[11] L. A. Passmore and T. T. Tang, "The long and short of it," Elife **10**, e70757 (2021).

[12] N. Biziaev, A. Shuvalov, A. Salman, T. Egorova, E. Shuvalova, and E. Alkalaeva, "The impact of mrna poly (a) tail length on eukaryotic translation stages," Nucleic acids research **52**, 7792–7808 (2024).

[13] A. Oh, S. Lee, H.-J. Park, S. Yoon, D. Ha, J. Lee, S. Lee, G. Roh, Y. Cho, S.-Y. Lee, *et al.*, "Loop structure in poly (a) tail of mrna vaccine enhances antigen translation efficiency and mrna stability," npj Vaccines **10**, 234 (2025).

[14] L. D. Fernandes, A. P. d. Moura, and L. Ciandrini, "Gene length as a regulator for ribosome recruitment and protein synthesis: theoretical insights," Scientific reports **7**, 17409 (2017).

[15] J. Paturej, S. S. Sheiko, S. Panyukov, and M. Rubinstein, "Molecular structure of bottlebrush polymers in melts," Science advances **2**, e1601478 (2016).

[16] D. Chatterjee and T. A. Vilgis, "Scaling laws of bottle-brush polymers in dilute solutions," Macromolecular Theory and Simulations **25**, 518–523 (2016).

[17] M. Alaboalirat, S. J. Scannelli, H. Rahmaninejad, J.-M. Carrillo, C. Do, J. B. Matson, and R. Ashkar, "Solution structure and scaling laws of cylindrical and tapered bottlebrush polymers," Macromolecules **56**, 9264–9276 (2023).

[18] K. Kremer and G. S. Grest, "Dynamics of entangled linear polymer melts: A molecular-dynamics simulation," The Journal of Chemical Physics **92**, 5057–5086 (1990).

[19] T. Guo, O. L. Modi, J. Hirano, H. V. Guzman, and T. Tsuboi, "Single-chain models illustrate the 3d rna folding shape during translation," Biophysical Reports **2** (2022).

[20] M. P. Howard, J. A. Anderson, A. Nikoubashman, S. C. Glotzer, and A. Z. Panagiotopoulos, "Efficient neighbor list calculation for molecular simulation of colloidal systems using graphics processing units," Computer Physics Communications **203**, 45–52 (2016).

[21] M. P. Howard, A. Statt, F. Madutsa, T. M. Truskett, and A. Z. Panagiotopoulos, "Quantized bounding volume hierarchies for neighbor search in molecular simulations on graphics processing units," Computational Materials Science **164**, 139–146 (2019).

[22] J. A. Anderson, J. Glaser, and S. C. Glotzer, "Hoomd-blue: A python package for high-performance molecular dynamics and hard particle monte carlo simulations," Computational Materials Science **173**, 109363 (2020).

[23] P. E. Rouse Jr, "A theory of the linear viscoelastic properties of dilute solutions of coiling polymers," The Journal of Chemical Physics **21**, 1272–1280 (1953).

[24] A.-b. Li, Y.-g. Yao, and H. Xu, "Stiffness and excluded volume effects on conformation and dynamics of polymers: A simulation study," Chinese Journal of Polymer Science **30**, 350–358 (2012).

[25] P.-G. De Gennes, *Scaling concepts in polymer physics* (Cornell university press, 1979).

[26] M. Doi, S. F. Edwards, and S. F. Edwards, *The theory of polymer dynamics*, Vol. 73 (oxford university press, 1988).

[27] H.-P. Hsu, "Monte carlo simulations of lattice models for single polymer systems," The Journal of chemical physics **141** (2014).

[28] L. Schäfer, A. Ostendorf, and J. Hager, "Scaling of the correlations among segment directions of a self-repelling polymer chain," Journal of Physics A: Mathematical and General **32**, 7875 (1999).

[29] J. Wittmer, H. Meyer, J. Baschnagel, A. Johner, S. Obukhov, L. Mattioni, M. Mueller, and A. N. Semenov, "Long range bond-bond correlations in dense polymer solutions," Physical review letters **93**, 147801 (2004).

[30] H.-P. Hsu, W. Paul, and K. Binder, "Standard definitions of persistence length do not describe the local "intrinsic" stiffness of real polymer chains," Macromolecules **43**, 3094–3102 (2010).

[31] C. P. Lindsey and G. D. Patterson, "Detailed comparison of the williams–watts and cole–davidson functions," The Journal of chemical physics **73**, 3348–3357 (1980).

[32] C. Xiao and D. M. Heyes, "Effects of bead-bead interactions on the static and dynamical properties of model polymer solutions," Physical Review E **60**, 5757 (1999).

[33] P. Mangeol, T. Bizebard, C. Chiaruttini, M. Dreyfus, M. Springer, and U. Bockelmann, "Probing ribosomal protein–rna interactions with an external force," Proceedings of the National Academy of Sciences **108**, 18272–18276 (2011).

[34] X. Qu, L. Lancaster, H. F. Noller, C. Bustamante, and I. Tinoco Jr, "Ribosomal protein s1 unwinds double-stranded rna in multiple steps," Proceedings of the National Academy of Sciences **109**, 14458–14463 (2012).

[35] C. T. A. Wong and M. Muthukumar, "Scaling theory of polymer translocation into confined regions," Biophysical journal **95**, 3619–3627 (2008).

[36] F. Vargas-Lara, S. M. Stavis, E. A. Strychalski, B. J. Nablo, J. Geist, F. W. Starr, and J. F. Douglas, "Dimensional reduction of duplex dna under confinement to nanofluidic slits," Soft Matter **11**, 8273–8284 (2015).

[37] N. Nahali, M. Oshaghi, and J. Paulsen, "Modeling properties of chromosome territories using polymer filaments in diverse confinement geometries," Chromosome Research **32**, 11 (2024).